

## 氰基桥联的 $\text{Fe}_2\text{Ni}_2$ 单分子磁体的合成与磁性

吴家起 孟银杉 朱海浪 矫成奇 刘涛\*  
(大连理工大学精细化工国家重点实验室,大连 116024)

**摘要:** 利用三氰基构筑单元  $\text{Bu}_4\text{N}[\text{Fe}^{\text{III}}(\text{PzTp})(\text{CN})_3]$  ( $\text{PzTp}$ =tetrakis(pyrazolyl)borate)和4,4'-二甲氧基-2,2'-联吡啶(4,4'-dmobpy)配体,合成了2例氰基桥联的 $\text{Fe}^{\text{III}}\text{Ni}^{\text{II}}_2$ 四核配合物。单晶X射线衍射表明化合物 $[\text{Fe}^{\text{III}}(\text{PzTp})(\text{CN})_3]_2[\text{Ni}^{\text{II}}_2(4,4'\text{-dmobpy})_4][\text{Fe}^{\text{III}}(\text{PzTp})(\text{CN})_3]_2 \cdot 2\text{CH}_3\text{OH}$  (**1**)和 $[\text{Fe}^{\text{III}}(\text{PzTp})(\text{CN})_3]_2[\text{Ni}^{\text{II}}_2(4,4'\text{-dmobpy})_4](\text{PF}_6)_2$  (**2**)具有四核四方分子结构。直流磁化率测试表明配合物**1**和**2**均表现为分子内的铁磁耦合作用。交流磁化率测试表明配合物**1**和**2**在零场下具有慢磁弛豫行为,有效能垒分别为12.8和13.0 K。

**关键词:** 氰基桥联; 单分子磁体; 铁磁耦合

中图分类号: O614.81<sup>+</sup>1; O614.7<sup>+</sup>11 文献标识码: A 文章编号: 1001-4861(2020)12-2331-09

DOI: 10.11862/CJIC.2020.252

## Synthesis and Magnetism of Cyano-bridged $\text{Fe}_2\text{Ni}_2$ Single-Molecule Magnets

WU Jia-Qi MENG Yin-Shan ZHU Hai-Lang JIAO Cheng-Qi LIU Tao\*

(State Key Laboratory of Fine Chemicals, Dalian University of Technology, Dalian, Liaoning 116024, China)

**Abstract:** Two cyano-bridged  $\text{Fe}_2\text{Ni}_2$  complexes were synthesized via the reaction of tricyanometallate building block  $\text{Bu}_4\text{N}[\text{Fe}^{\text{III}}(\text{PzTp})(\text{CN})_3]$  ( $\text{PzTp}$ =tetrakis(pyrazolyl)borate) and 4,4'-dimethoxy-2,2'-bipyridine (4,4'-dmobpy) ligand. X-ray diffraction study reveals that complexes  $[\text{Fe}^{\text{III}}(\text{PzTp})(\text{CN})_3]_2[\text{Ni}^{\text{II}}_2(4,4'\text{-dmobpy})_4][\text{Fe}^{\text{III}}(\text{PzTp})(\text{CN})_3]_2 \cdot 2\text{CH}_3\text{OH}$  (**1**) and  $[\text{Fe}^{\text{III}}(\text{PzTp})(\text{CN})_3]_2[\text{Ni}^{\text{II}}_2(4,4'\text{-dmobpy})_4](\text{PF}_6)_2$  (**2**) exhibit a tetranuclear square structure. Direct current susceptibility measurements indicate that **1** and **2** show intramolecular ferromagnetic interactions between  $\text{Fe}(\text{III})$  and  $\text{Ni}(\text{II})$  ions. Complexes **1** and **2** show the magnetic relaxation property in the absence of dc field, behaving as single-molecule magnets. The fitted relaxation energy barrier  $E_a/k_B$  for **1** and **2** were 12.8 and 13.0 K, respectively. CCDC: 1988983, **1**; 1988982, **2**.

**Keywords:** cyano-bridged; single-molecule magnet; ferromagnetic interaction

## 0 Introduction

Since the discovery of a  $\text{Mn}_{12}$ -Ac cluster ( $[\text{Mn}_{12}\text{O}_{12}(\text{CH}_3\text{COO})_{16}(\text{H}_2\text{O})_{24}] \cdot 2\text{CH}_3\text{COOH} \cdot 4\text{H}_2\text{O}$ ) showing the magnet-like behavior in 1993, researchers have put a lot of effort in the field of molecular magnetism<sup>[1-2]</sup>. Unlike the traditional bulk magnets, such type of molecular materials, also known as single-molecule

magnets (SMMs), can exhibit slow relaxation of magnetization, hysteresis and quantized behaviors at molecular level, showing promising applications in high-density information storage, quantum computing and spintronic devices<sup>[3-10]</sup>. These exceptional properties have also attracted considerable interest in the fundamental scientific studies. For transition metal based SMMs, the non-spherical crystal field removes the degeneracy

收稿日期: 2020-03-14。收修改稿日期: 2020-08-03。

国家自然科学基金(No.21871039, 21801037, 91961114, 21903011, 21421005)资助项目。

\*通信联系人。E-mail: liutao@dlut.edu.cn

of ground multiplet, generating a double-well potential system. When the molecules were magnetically polarized by external field, the reversal of magnetic moment needs to climb the sub energy levels to reach the opposite site and overcome the spin reversal barrier<sup>[2]</sup>. This barrier is crucial for the long-time memory property, which is governed by the zero-field splitting parameter and ground spin number ( $U_{\text{eff}}=|D|S^2$  for integer system;  $U_{\text{eff}}=|D|(S^2-1/4)$  for half-integer system). In the early studies, researchers designed a number of high-nuclear transition-metal-based clusters with large ground spin number<sup>[11-18]</sup>. However, due to the cancelation of magnetic anisotropy of individual metal ions, the overall magnetic anisotropy of these clusters is usually small, resulting in small energy barriers. Nevertheless, the study of these molecular clusters with a wide variety of spin topologies and architectures provides a good platform to better understand the magneto-structural correlations. Another strategy is to improve the uniaxial anisotropy by introducing lanthanide ions or anisotropic transition-metal-based building blocks<sup>[11,17,19]</sup>. Among them, the metallocyanide building blocks show the priority in constructing new SMMs<sup>[12,20-21]</sup>. The cyanide bridge shows not only the ability of transmitting magnetic exchange interaction, but also the ease of molecular design through step-by-step synthetic approach<sup>[22-23]</sup>. A typical example is the  $[\text{Mo}(\text{CN})_7]^{4-}$ -based trinuclear  $\text{Mn}_2\text{Mo}$  molecule that exhibited the highest energy barrier among the cyanide-based SMMs<sup>[10]</sup>. More importantly, these metallocyanide building blocks are essential for the metal-to-metal electron transfer, spin-crossover, magneto-optic and magneto-electric properties<sup>[24-25]</sup>. With this in mind, we aim to design square-type cyano-bridged SMMs. Metallocyanate building block  $\text{Bu}_4\text{N}[\text{Fe}^{\text{III}}(\text{PzTp})(\text{CN})_3]$  (PzTp=tetrakis(pyrazolyl)borate) was chosen to react with Ni(II) ion, as it features larger spin-orbit coupling among 3d transition metal ions and usually shows the ferromagnetic interactions between the low-spin (LS) Fe(III) and high-spin (HS) Ni(II) ions<sup>[26]</sup>. Herein, we report the synthesis, crystal structures and magnetic properties of  $[\text{Fe}^{\text{III}}(\text{PzTp})(\text{CN})_3]_2[\text{Ni}^{\text{II}}_2(4,4'\text{-dmobpy})_4][\text{Fe}^{\text{III}}(\text{PzTp})(\text{CN})_3]_2 \cdot 2\text{CH}_3\text{OH}$  (**1**) and  $[\text{Fe}^{\text{III}}(\text{PzTp})(\text{CN})_3]_2[\text{Ni}^{\text{II}}_2(4,4'\text{-dmobpy})_4]$

$(\text{PF}_6)_2$  (**2**) ( $4,4'$ -dmobpy= $4,4'$ -dimethoxy- $2,2'$ -bipyridine). Both of them exhibit the SMM behaviors.

## 1 Experimental

### 1.1 Materials and general methods

All chemical reagents were purchased from commercial sources and used without further purification.  $\text{Bu}_4\text{N}[\text{Fe}^{\text{III}}(\text{PzTp})(\text{CN})_3]$  were synthesized according to the literature method<sup>[27-28]</sup> and the  $4,4'$ -dimethoxy- $2,2'$ -bipyridine ligand was acquired from commercial source. Elemental analyses were performed on an Elementar Vario EL III analyzer. Magnetic measurements of the samples were performed on a Quantum Design SQUID (MPMSXL-7) magnetometer and Quantum Design PPMS-9. Data were corrected for the diamagnetic contribution from holders and molecules using Pascal constants.

### 1.2 Synthesis of 1

An aqueous solution of  $\text{NiCl}_2 \cdot 6\text{H}_2\text{O}$  (0.005 mmol, 0.5 mL) was placed at the bottom of a test tube. A mixture of methanol and water (1 : 1, V/V, 3 mL) was gently layered on the top of the solution, and then the methanol solution of  $\text{Bu}_4\text{N}[\text{Fe}^{\text{III}}(\text{PzTp})(\text{CN})_3]$  (0.005 mmol, 0.5 mL) and  $4,4'$ -dmobpy (0.01 mmol) was carefully added as the third layer. After one month, red block crystals were obtained, then were collected after washing with water and drying in the air. Yield: 33% based on  $\text{NiCl}_2 \cdot 6\text{H}_2\text{O}$ . Anal. Calcd. for  $\text{C}_{110}\text{H}_{106}\text{B}_4\text{Fe}_4\text{N}_{52}\text{Ni}_2\text{O}_{10}$ (%): C 48.93, H 3.96, N 26.97; Found(%): C 48.07, H 3.64, N 26.91.

### 1.3 Synthesis of 2

Complex **2** was synthesized with the similar procedure of complex **1**, except using a methanol solution of  $\text{Bu}_4\text{N}[\text{Fe}^{\text{III}}(\text{PzTp})(\text{CN})_3]$  (0.005 mmol, 0.5 mL),  $4,4'$ -dmobpy (0.01 mmol) and  $\text{NH}_4\text{PF}_6$  (0.005 mmol) as the third layer. Yield: 30% based on  $\text{NiCl}_2 \cdot 6\text{H}_2\text{O}$ . Anal. Calcd. for  $\text{C}_{78}\text{H}_{72}\text{B}_2\text{F}_{12}\text{Fe}_2\text{N}_{30}\text{Ni}_2\text{O}_8\text{P}_2$ (%): C 44.61, H 3.43, N 20.01; Found(%): C 44.36, H 3.47, N 19.78.

### 1.4 X-ray crystallography

The diffraction data were collected on Bruker D8 Venture CMOS-based diffractometer (Mo  $K\alpha$  radiation,  $\lambda=0.071\ 073$  nm) using APEX3<sup>[29]</sup> program at 293 and 120 K for complexes **1** and **2**, respectively. Final unit

cell parameters were obtained based on all observed reflections from integration of all frame data. All crystallographic structures were solved by direct methods and refined with SHELXL-2015 implanted in the Olex 2 program package<sup>[30-31]</sup>. For complexes **1** and **2**, all non-hydrogen atoms were refined anisotropically. The

hydrogen atoms of organic ligands were located geometrically and fixed with isotropic thermal parameters. The details of the structure refinement for complexes **1** and **2** are summarized in Table 1.

CCDC: 1988983, **1**; 1988982, **2**.

**Table 1** Crystal data and structure refinements for complexes **1** and **2**

Complex	<b>1</b>	<b>2</b>
Formula	C <sub>110</sub> H <sub>106</sub> B <sub>4</sub> Fe <sub>4</sub> N <sub>52</sub> Ni <sub>2</sub> O <sub>10</sub>	C <sub>78</sub> H <sub>72</sub> B <sub>2</sub> F <sub>12</sub> Fe <sub>2</sub> N <sub>30</sub> Ni <sub>2</sub> O <sub>8</sub> P <sub>2</sub>
Formula weight	2 700.52	2 098.33
Crystal system	Triclinic	Monoclinic
Space group	$P\bar{1}$	$P2_1/n$
<i>a</i> / nm	1.425 22(6)	1.264 64(11)
<i>b</i> / nm	1.594 29(6)	2.418 87(18)
<i>c</i> / nm	1.633 75(6)	1.549 72(12)
$\alpha$ / (°)	62.807 0(10)	
$\beta$ / (°)	68.328(2)	95.280(3)
$\gamma$ / (°)	76.615(2)	
<i>V</i> / nm <sup>3</sup>	3.059 7(2)	4.720 5(7)
<i>Z</i>	1	2
<i>D<sub>c</sub></i> / (g·cm <sup>-3</sup> )	1.466	1.476
<i>F</i> (000)	1 390.0	2 140.0
Reflection collected	55 553	42 731
Unique reflection ( <i>R</i> <sub>int</sub> )	10 709 (0.061 1)	10 832 (0.061 0)
Goodness-of-fit on <i>F</i> <sup>2</sup>	1.075	1.032
Final <i>R</i> indices <sup>a,b</sup> [ <i>I</i> > 2σ( <i>I</i> )]	<i>R</i> <sub>1</sub> =0.048 1, <i>wR</i> <sub>2</sub> =0.119 2	<i>R</i> <sub>1</sub> =0.048 6, <i>wR</i> <sub>2</sub> =0.115 0
<i>R</i> indices <sup>a,b</sup> (all data)	<i>R</i> <sub>1</sub> =0.079 8, <i>wR</i> <sub>2</sub> =0.131 6	<i>R</i> <sub>1</sub> =0.083 9, <i>wR</i> <sub>2</sub> =0.130 6

$$^a R_1 = \sum (|F_o| - |F_c|) / \sum |F_o|; ^b wR_2 = [\sum w(|F_o| - |F_c|)^2 / \sum wF_o^2]^{1/2}.$$

## 2 Results and discussion

### 2.1 Crystal structures of **1** and **2**

Single-crystal X-ray diffraction analysis reveals that **1** crystallizes in the triclinic space group  $P\bar{1}$ . As shown in Fig. 1a, **1** exhibits a tetranuclear square structure. Two uncoordinated methanol molecules are located between the clusters. Within the molecule, each [Fe<sup>III</sup>(PzTp)(CN)<sub>3</sub>]<sup>-</sup> fragment is alternatively connected with two [Ni(4,4'-dmobpy)<sub>2</sub>]<sup>2+</sup> entities through two of its three cyanide groups, forming a {Fe<sub>2</sub>(μ-CN)<sub>4</sub>Ni<sub>2</sub>} tetranuclear square structure. The Fe(III) ion adopts a slightly distorted octahedron coordination environment, which is composed of three cyanide carbon atoms and three pyrazole nitrogen atoms. The Fe-C<sub>cyanide</sub> and Fe-N<sub>PzTp</sub> bond lengths are 0.192 9(4) and 0.195 9(3)~0.198 1(3)

nm, respectively. The bond lengths are in good agreement with the low-spin (LS) Fe(III) complexes reported previously<sup>[32-34]</sup>. The Ni-N<sub>dmobpy</sub> bond distances (0.205 2(3)~0.209 9(3) nm) are also in agreement with the high-spin (HS) Ni(II) complexes. The Fe-C≡N bond angles (173.8(3)°~174.6(3)°) show good linearity. Within the unit of [Ni(4,4'-dmobpy)<sub>2</sub>]<sup>2+</sup>, each Ni(II) ion is also located in an octahedral environment with four nitrogen atoms from two 4,4'-dmobpy ligands and two cyanide nitrogen atoms. Different from the [Fe<sup>III</sup>(PzTp)(CN)<sub>3</sub>]<sup>-</sup> building block, the Ni-N≡C bond angles (146.0(3)°~149.5(3)°) show significant deviation from linearity, which will influence the magnitude of the magnetic interactions. There are an intermolecular edge-to-face C-H...π interactions between C19-H19A and pyrazole rings (0.327 49(1) nm) and an intermolecular offset face

-to-face  $\pi \cdots \pi$  interactions between adjacent pyrazole rings (centroid distance: 0.401 36(1) nm, dihedral angle: 20.9(6) $^\circ$ ). The neighboring molecules are further linked through above intermolecular stacking interactions to form a 2D supramolecular layer (Fig. 1b). The shortest distances of intramolecular Fe $\cdots$ Ni, Fe $\cdots$ Fe, and Ni $\cdots$ Ni are 0.495 85(10), 0.651 29(9) and 0.745 13(7) nm, respectively. The nearest intermolecular distances of Fe $\cdots$ Ni, Fe $\cdots$ Fe, and Ni $\cdots$ Ni are 1.269 07(1), 0.996 16(9) and 1.193 95(9) nm, respectively.

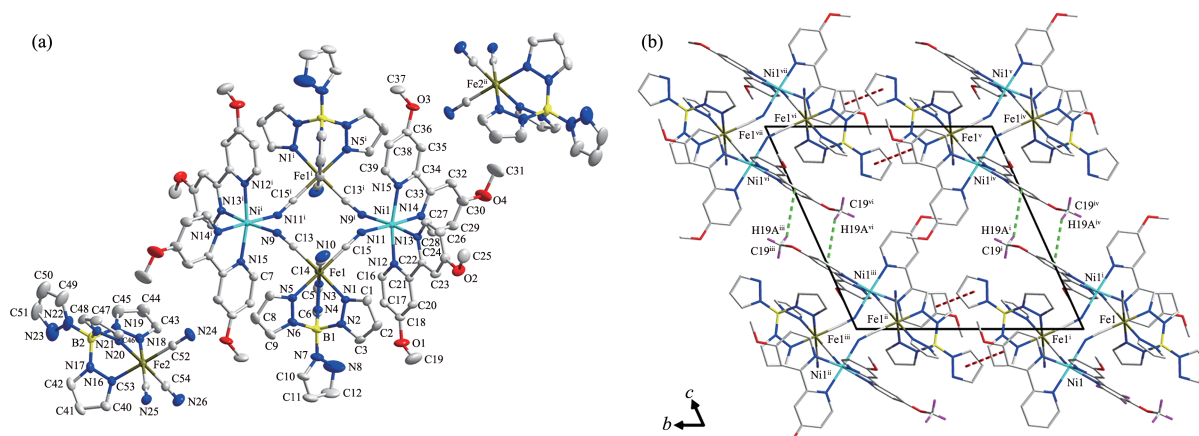


Fig.1 (a) Unit structure of **1** with 30% thermal ellipsoids probability, where all hydrogen atoms are omitted for clarity and atomic scheme is: dark yellow for Fe, turquoise for Ni, gray for C, blue for N, yellow for B; Symmetry codes:  $^i -x, -y, -z$ ;  $^{ii} x, -1+y, z$ ; (b) Packing diagram of **1** illustrating  $\pi \cdots \pi$  and C-H $\cdots$  $\pi$  contacts in  $bc$  plane; Symmetry codes:  $^i -1+x, 1+y, z$ ;  $^{ii} -1-x, 2-y, -z$ ;  $^{iii} -1+x, 2+y, z$ ;  $^{iv} -1-x, 1-y, 1-z$ ;  $^v -1+x, 1+y, 1+z$ ;  $^{vi} -1-x, 2-y, 1-z$ ;  $^{viii} -1+x, 2+y, 1+z$

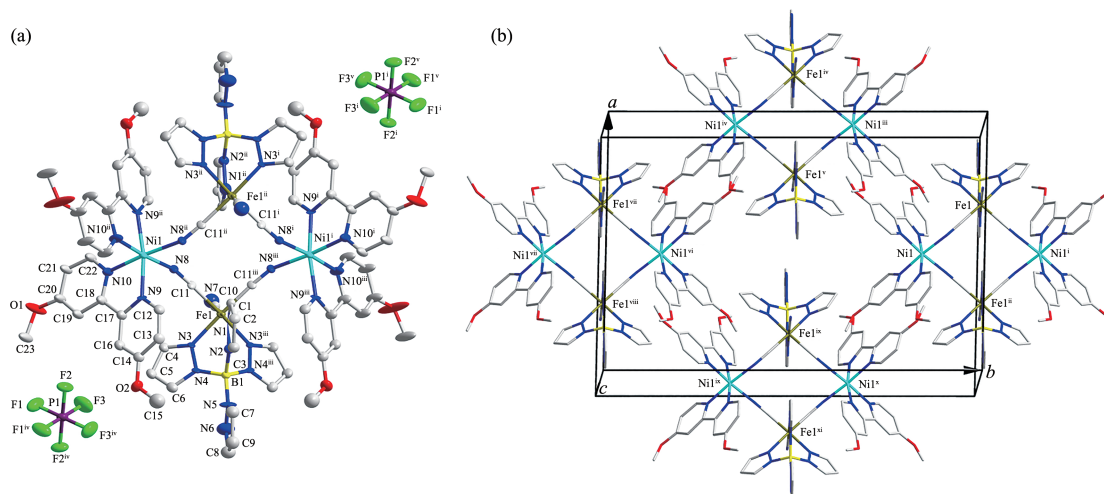


Fig.2 (a) Unit structure of **2** with 30% thermal ellipsoids probability, where all hydrogen atoms are omitted for clarity and atomic scheme is: dark yellow for Fe, turquoise for Ni, gray for C, blue for N, violet for P, bright green for F, yellow for B; Symmetry code:  $^i 1-x, 2-y, 1-z$ ;  $^{ii} 1-x, y, 1-z$ ;  $^{iii} x, 2-y, z$ ;  $^{iv} 2-x, y, 2-z$ ;  $^v -1+x, 2-y, -1+z$ ; (b) Packing diagram of **2** in  $ab$  plane; Symmetry codes:  $^i 1-x, 2-y, 1-z$ ;  $^{ii} 1-x, y, 1-z$ ;  $^{iii} 3/2-x, 3/2-y, 1-z$ ;  $^{iv} 1/2+x, -1/2+y, z$ ;  $^v 3/2-x, -1/2+y, 1-z$ ;  $^{vi} 1-x, 1-y, 1-z$ ;  $^{vii} x, -1+y, z$ ;  $^{viii} 1-x, -1+y, 1-z$ ;  $^{ix} -1/2+x, -1/2+y, z$ ;  $^x 1/2-x, 3/2-y, 1-z$ ;  $^{xi} 1/2-x, -1/2+y, 1-z$

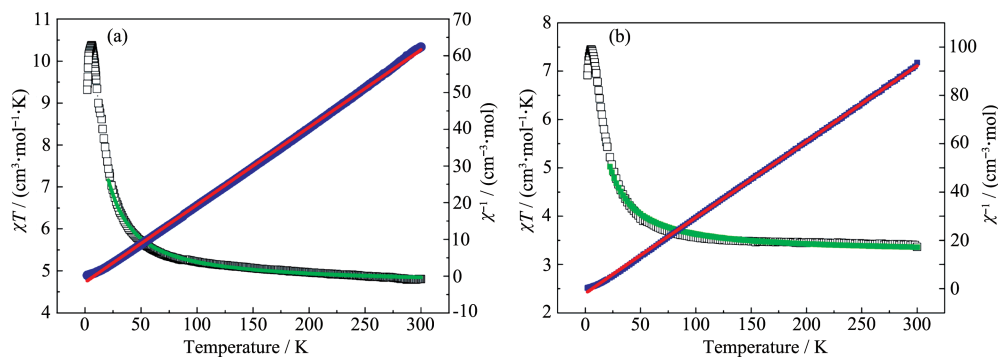
Different from complex **1**, single-crystal X-ray diffraction analysis reveals that **2** crystallizes in the monoclinic space group  $P2_1/n$ . Complex **2** is composed of a  $\{[\text{Fe}^{\text{III}}(\text{PzTp})(\text{CN})_3]_2\text{Ni}^{\text{II}}(4,4'\text{-dmobpy})_4\}^{2+}$  square and two  $\text{PF}_6^-$  counterions (Fig. 2a). Each Fe(III) center also adopts a slightly distorted octahedral geometry with three N atoms from pyrazoles and three cyanide carbon atoms. The average Fe-C<sub>cyanide</sub> and Fe-N<sub>PzTp</sub> bond lengths are 0.192 2(4) nm and 0.196 1(2)~0.198 1(3) nm, respectively. The Ni-N<sub>dmobpy</sub> bond lengths and Ni-N

$\equiv\text{C}$  angles in **2** are 0.206 2(2)~0.208 3(2) nm and 147.8(2)°~151.4(2)°, respectively, which are slightly different from **1**. The intramolecular Fe $\cdots$ Ni (0.493 38(36) nm) and Fe $\cdots$ Fe (0.632 84(56) nm) distances are shorter than those of complex **1**, but the Ni $\cdots$ Ni distance (0.757 10(56) nm) is a little longer. The nearest intermolecular Fe $\cdots$ Ni, Fe $\cdots$ Fe and Ni $\cdots$ Ni distances are 1.293 74(55), 0.939 87(54) and 1.542 03(63) nm, respectively. However, the nearest offset face-to-face stacking interactions between the pyridine rings (C18, C19, C20, C21, C22, and N10) in adjacent 4,4'-dmobpy ligands (dihedral angle: 0.0(1)°) with a centroid-centroid distance is 0.44 92(1) nm, excluding the existence of  $\pi\cdots\pi$  stacking interactions (Fig.2b).

## 2.2 Magnetic property

Magnetic susceptibility data were collected under 1 kOe dc field in a temperature range of 2~300 K (Fig.3). The  $\chi T$  values for **1** and **2** were 4.81 and 3.36  $\text{cm}^3\cdot\text{mol}^{-1}\cdot\text{K}$  at 300 K, respectively. The  $\chi T$  value of **2** is in the typical range for two uncorrelated LS Fe(III) ions ( $S=1/2$ ) and two HS Ni(II) ions ( $S=1$ )<sup>[35]</sup>. The larger  $\chi T$  value of complex **1** is attributed to contribution from the paramagnetic  $[\text{Fe}^{\text{III}}(\text{PzTp})(\text{CN})_3]^-$  counterions. For complex **1**, the  $\chi T$  value gradually increased as the temperature was lowered to 100 K, then increased rapidly to the maximum value of 10.38  $\text{cm}^3\cdot\text{mol}^{-1}\cdot\text{K}$  at 5.7 K, followed by a decrease to 9.31  $\text{cm}^3\cdot\text{mol}^{-1}\cdot\text{K}$  at 2 K. Such a decrease is probably due to the zero-field splitting of Ni(II) ions or intermolecular antiferromagnetic interactions. The increasing of  $\chi T$  values suggests the existence of intramolecular ferromagnetic interactions between Fe(III) and Ni(II) ions. To verify this, the

Curie-Weiss law  $\chi=C/(T-\theta)$  was applied to fit the  $\chi^{-1}$  vs  $T$  plots, resulting the Curie constant  $C$  of 4.74  $\text{cm}^3\cdot\text{mol}^{-1}\cdot\text{K}$  and Weiss temperature  $\theta$  of 7.80 K. The positive Weiss temperature indicates the ferromagnetic interactions between the paramagnetic centers in complex **1**<sup>[25]</sup>. For complex **2**, the plots of  $\chi T$  versus temperature were different from that of **1**, which showed a slightly decrease when decreasing the temperature to 120 K. The  $\chi T$  values experienced an upturn upon further cooling, reaching a maximum value of 7.45  $\text{cm}^3\cdot\text{mol}^{-1}\cdot\text{K}$  at 5.5 K. The  $\chi T$  value at 2 K is 6.92  $\text{cm}^3\cdot\text{mol}^{-1}\cdot\text{K}$ . The magnetic data followed the Curie-Weiss law in the temperature range of 2~300 K with a positive Weiss temperature  $\theta$  of 6.13 K and Curie constant  $C$  of 3.19  $\text{cm}^3\cdot\text{mol}^{-1}\cdot\text{K}$ . It is noteworthy that the Weiss temperature of complex **2** was smaller than that of **1**, suggesting a smaller intramolecular ferromagnetic interaction in **2**. To further demonstrate the intramolecular interactions, the susceptibilities were fitted with the following Hamiltonian  $H=-2J[S_{\text{Fe}^{\text{I}}}(S_{\text{Ni}^{\text{I}}+S_{\text{Ni}^{\text{II}}})+S_{\text{Fe}^{\text{II}}}(S_{\text{Ni}^{\text{I}}+S_{\text{Ni}^{\text{II}}})]$ , where  $J$  is the coupling parameter,  $S_{\text{Fe}}$  is 1/2 and  $S_{\text{Ni}}$  is 1. For complex **1**, the  $\chi T$  versus  $T$  plots above 20 K can be well fitted with the following parameters:  $g_{\text{Fe}}=2.32$ ,  $g_{\text{Ni}}=2.29$  and  $J=6.83 \text{ cm}^{-1}$ . The positive coupling parameter further confirms the ferromagnetic interaction between Fe<sup>III</sup><sub>LS</sub> and Ni<sup>II</sup><sub>HS</sub> ions. While for complex **2**, the coupling parameter (5.65  $\text{cm}^{-1}$ ) was smaller than that of complex **1** (6.83  $\text{cm}^{-1}$ ), and the  $g$  factor for Ni<sup>II</sup><sub>HS</sub> ions (2.11) also showed a smaller magnitude. The variable-field magnetization measurements were also performed at 1.8 K. As shown in Fig.4, the isothermal magnetizations of **1** and **2** first increased lin-



Red lines represent the Curie-Weiss fitting, and the green lines represent the fitting with exchange coupling Hamiltonian

Fig.3 Temperature-dependence magnetic susceptibility of **1** (a) and **2** (b)

early and then increased gradually, reaching a maximum value of  $7.61N\beta$  and  $6.04N\beta$  at 50 kOe, respectively. The magnetization value of **1** was higher than that of **2** because the former complex contains two additional paramagnetic counter anions. It should be noted that the magnetization value of complex **1** was not saturated even at 50 kOe, suggesting the significant magnetic anisotropy from Fe(III) and Ni(II) ions. Moreover, the zero-field-cooled (ZFC) and field-cooled magnetization plots (FC) under a field of 100 Oe for **1** and **2** showed no divergence (Fig. 5), therefore excluding the spontaneous magnetization above 1.8 K.

The temperature dependence of the ac magnetic susceptibility for **1** and **2** were also investigated under 5 Oe alternating current (ac) field and zero direct current (dc) field to probe the dynamics of the magnetization. As shown in Fig. 6, a clear frequency-dependent behavior of both the in-phase ( $\chi'$ ) and out-of-phase ( $\chi''$ ) signals was observed below 4 K, indicating the existence of slow magnetic relaxation. However, the maxima peaks of the out-of-phase signals did not ap-

pear. As a consequence, the relaxation times cannot be directly extracted. To evaluate the SMM performance, the generalized Debye model<sup>[26]</sup> was used to extract the energy barrier based on the relationship of  $\ln(\chi''/\chi') = \ln(\omega\tau_0) + E_a/(k_B T)$ , where  $\omega$  is  $2\pi f$ ,  $\tau_0$  is the pre-exponential factor and  $E_a$  is the energy barrier. The obtained energy barriers  $E_a/k_B$  was 12.8 K for complex **1** with  $\tau_0$  of 0.415  $\mu\text{s}$  (Fig. 7). Interestingly, complex **2** showed a similar barrier of 13.0 K. Meanwhile, the  $\tau_0$  value (0.154  $\mu\text{s}$ ) was smaller than that of **1**.

Although complex **1** shows stronger intramolecular ferromagnetic coupling and magnetic anisotropy of Ni(II) ions, its SMM performance is almost the same with complex **2**. This inspired us to further check the structural differences of them. Ferromagnetic interactions are found in complexes **1** and **2**, which can be rationalized according to the orthogonality of magnetic orbitals of the low-spin Fe(III) and high-spin Ni(II) ions<sup>[26]</sup>. The biggest structural difference lies on that complex **1** has two paramagnetic counterions while in complex **2** is diamagnetic one. The  $\pi \cdots \pi$  stacking

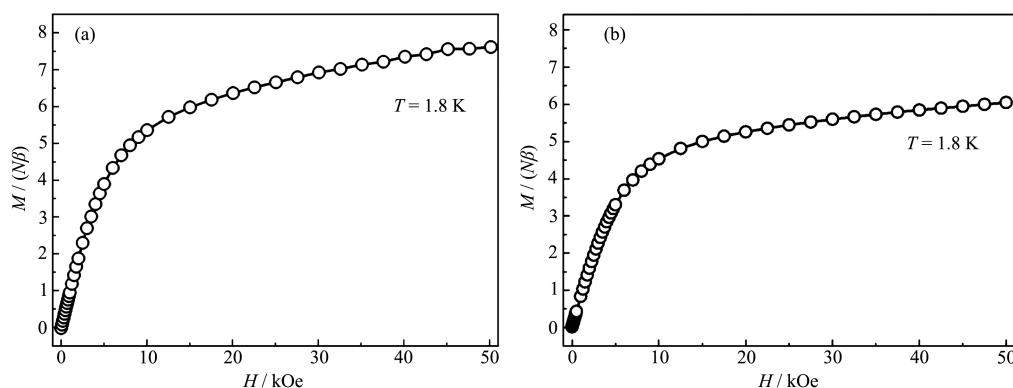


Fig. 4 Field-dependent magnetizations of **1** (a) and **2** (b) at 1.8 K

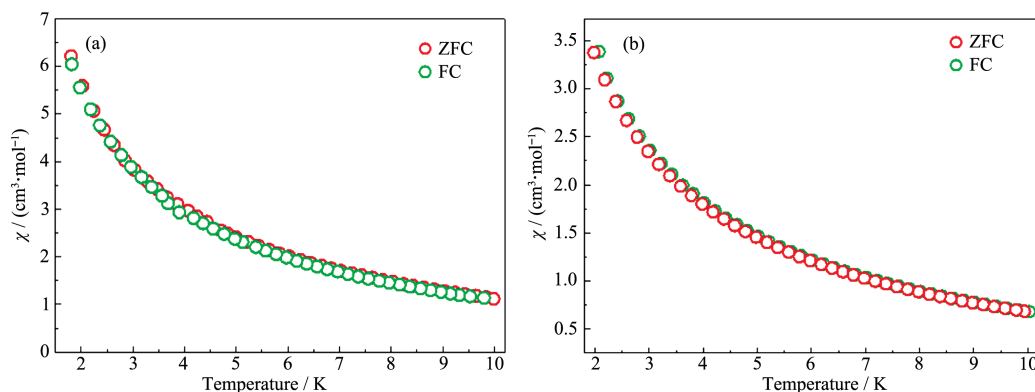


Fig. 5 Zero-field-cooled magnetization (ZFC) and field-cooled magnetization (FC) curves for **1** (a) and **2** (b) under 100 Oe dc field

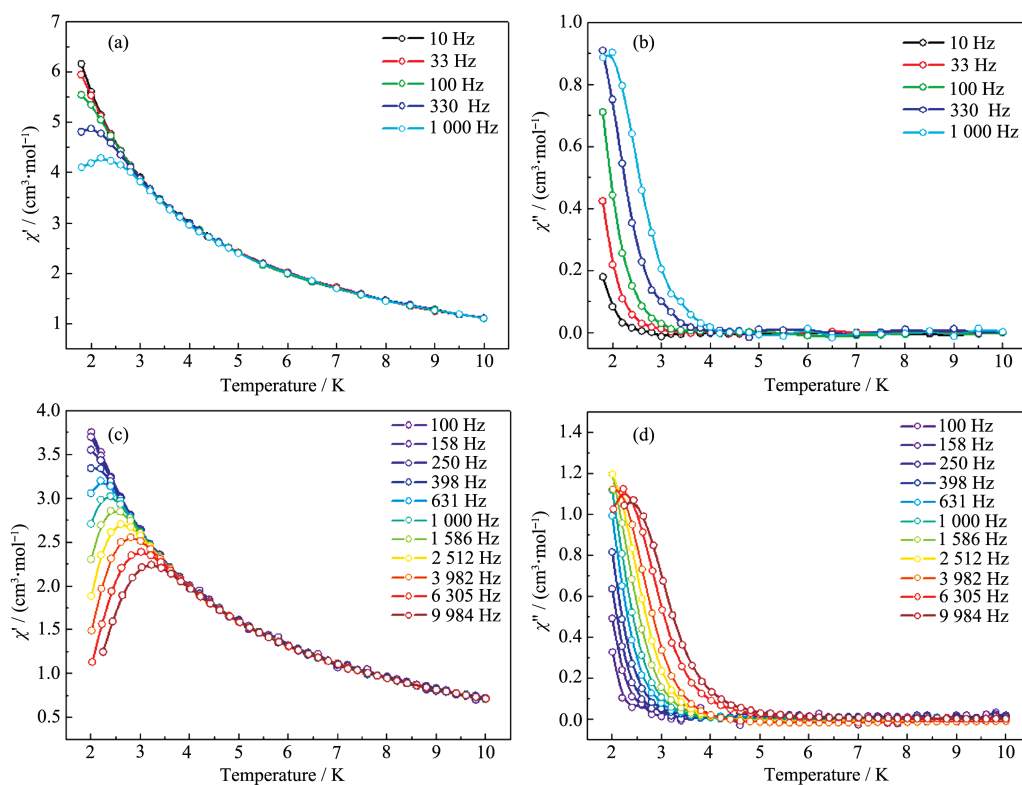
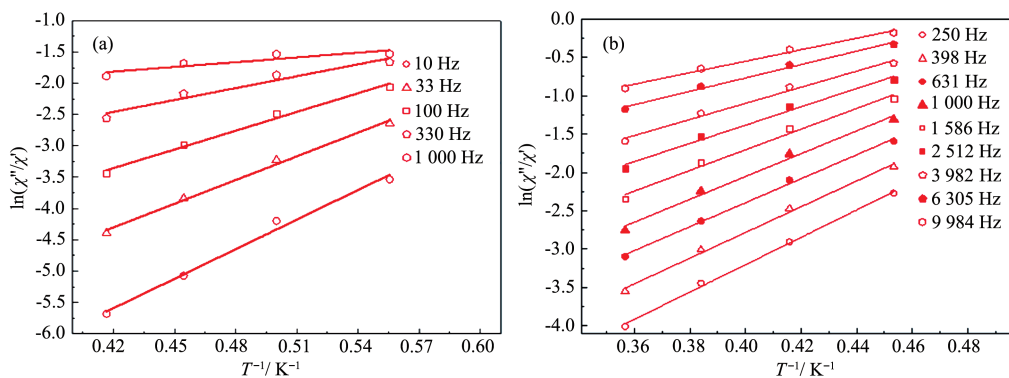


Fig.6 Frequency dependence of ac magnetic signals for complexes **1** (a:  $\chi'$ , b:  $\chi''$ ) and **2** (c:  $\chi'$ , d:  $\chi''$ ) at  $H_{ac}=5$  Oe and  $H_{dc}=0$  Oe



Solid line represented the fitting results over the temperature range of 1.8~2.4 K

Fig.7 Plots of  $\ln(\chi''/\chi')$  vs  $1/T$  of complexes **1** (a) and **2** (b)

interactions are found in complex **1**. The nearest intermolecular Ni $\cdots$ Ni distance (1.193 95(9) nm) is smaller than that of complex **2** (1.542 03(63) nm). This may lead to stronger intermolecular antiferromagnetic interactions in complex **1**. The coordination environments of Fe(III) sites do not show significant difference, as indicated by the Fe-C $\equiv$ N angles. This result is also reflected by the similar  $g$  factors for **1** (2.32) and **2** (2.34). According to the previous study, large Ni-N $\equiv$ C angle prefers stronger ferromagnetic interactions and conse-

quently better SMM performance. Complex **2** only shows slightly larger Ni-N $\equiv$ C angles. To further verify the magneto-structural correlations, the geometry analysis was applied to see the deviation from ideal octahedron of Ni(II) and Fe(III) coordination environments for complexes **1** and **2** and compared them with reported  $\{\text{Fe}^{\text{III}}_2\text{Ni}^{\text{II}}_2\}$  complexes (Table 2). As shown in Fig. 8a, the larger deviations from ideal octahedron environment for Ni(II) ion are correlated with smaller energy barriers in most cases. This intuitive conclusion is not

**Table 2 Relationship between structural parameters and energy barrier  $\Delta E/k_B$  of **1** and **2** and reported  $\{\text{Fe}^{\text{III}}_2\text{Ni}^{\text{II}}_2\}$  complexes**

Complex	$\angle\text{Fe}-\text{C}\equiv\text{N} / (^\circ)$	$\text{CShM}_{\text{Fe}}^{\text{a}}$	$\angle\text{Ni}-\text{N}\equiv\text{C} / (^\circ)$	$\text{CShM}_{\text{Ni}}^{\text{b}}$	$\Delta E/k_B / \text{K}$
<b>1</b>	173.8(3)~174.6(3)	0.092	146.0(3)~149.5(3)	0.929	12.8
<b>2</b>	173.4(3)~175.1(3)	0.089	147.8(2)~151.4(2)	0.892	13.0
<b>3</b> <sup>[37]</sup>	174.6(4)~177.4(4)	0.16	161.7(3)~173.8(3)	0.597	18.9
<b>4</b> <sup>[37]</sup>	174.7(2)~178.2(2)	0.234	169.8(2) or 171.7(2)	0.605	47.4
<b>5</b> <sup>[38]</sup>	173.4(4)~178.1(4)	0.228	167.1(4) or 171.9(3)	0.74	20.4
<b>6</b> <sup>[39]</sup>	173.6(4)~177.8(4)	0.079	160.3(4)~173.0(4)	0.696	17.5
<b>7</b> <sup>[39]</sup>	177.0(9)~178.5(9)	0.126	161.6(8)~177.2(8)	0.77	20.6
<b>8</b> <sup>[39]</sup>	174.8(4)~178.0(4)	0.102	164.7(4)~175.2(4)	0.597	20.8
<b>9</b> <sup>[34]</sup>	176.7(2)~178.1(2)	0.161	173.5(3) or 174.2(2)	0.762	15.7
<b>10</b> <sup>[25]</sup>	173.6(6)~178.5(7)	0.227	165.5(6) or 174.6(6)	0.627	64.3
<b>11</b> <sup>[25]</sup>	177.9(5)~179.5(4)	0.109	167.2(4)~170.3(3)	0.607	24.5
<b>12</b> <sup>[35]</sup>	175.1(8)~178.8(1)	0.124	152.5(8)~166.4(7)	0.68	65.1
<b>13</b> <sup>[40]</sup>	173.8(4)~179.5(5)	0.092 or 0.069	157.1(3)~171.5(3)	0.704 or 0.859	68.9
<b>14</b> <sup>[40]</sup>	172.2(1)~177.7(2)	0.091 or 0.113	157.5(1)~165.0(1)	0.955 or 0.690	12.6
<b>15</b> <sup>[41]</sup>	174.1(6)~176.2(6)	0.177	166.2(5)~170.6(5)	0.177	62.3

<sup>a</sup>  $\text{CShM}_{\text{Fe}}$ : continuous shape measure relative to ideal octahedron of  $\text{Fe}(\text{III})$  center; <sup>b</sup>  $\text{CShM}_{\text{Ni}}$ : continuous shape measure relative to ideal octahedron of  $\text{Ni}(\text{II})$  center.

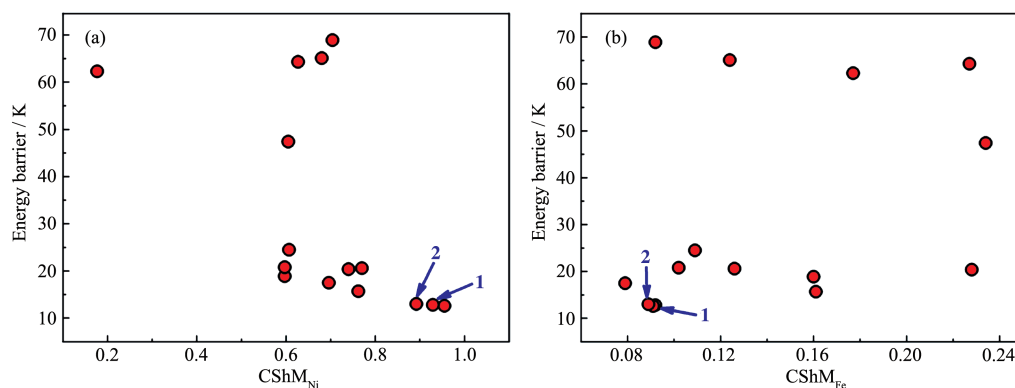


Fig.8 Correlations between energy barriers and parameters of  $\text{CShM}_{\text{Ni}}$  (a) and  $\text{CShM}_{\text{Fe}}$  (b)

applicable to the relation between  $\text{CShM}_{\text{Fe}}$  parameter (continuous shape measure relative to ideal octahedron of  $\text{Fe}(\text{III})$  center) and energy barrier (Fig.8b). It is probably due to the rigid structure of the  $[\text{Fe}^{\text{III}}(\text{PzTp})(\text{CN})_3]^-$  building block, which shows a small variation for the  $\text{CShM}_{\text{Fe}}$  parameter (0.089~0.234). Besides of these, the non-linear character of the  $\text{Fe}-\text{C}\equiv\text{N}$  and  $\text{Ni}-\text{N}\equiv\text{C}$  angles may also have some effects on the intramolecular interactions, which in turn influence the ground spin state and energy barriers. In addition, it can be noted that the  $\text{CShM}$  values of  $\text{Fe}(\text{III})$  and  $\text{Ni}(\text{II})$  for complex **1** are slightly higher than that of **2**. This indicates that the  $\text{Ni}(\text{II})$  ions are located in a more distorted octahedron

environment. This may provide a compensation to the smaller coupling interactions in **2**, resulting similar SMM performance of **1** and **2**.

### 3 Conclusions

In summary, two new cyano-bridged  $\text{Fe}^{\text{III}}_2\text{Ni}^{\text{II}}_2$  tetranuclear square complexes were synthesized by using the  $\text{Bu}_4\text{N}[\text{Fe}^{\text{III}}(\text{PzTp})(\text{CN})_3]$  as building block and 4,4'-dimethoxy-2,2'-bipyridine as ancillary ligand. Single-crystal X-ray diffraction analysis reveal that complexes **1** and **2** exhibit similar  $\text{Fe}^{\text{III}}_2\text{Ni}^{\text{II}}_2$  clusters but with different counterions. Magnetic measurements indicate that both complexes **1** and **2** exhibit intramolecular

ferromagnetic interactions. However, their single-molecular magnetic performances are modest, showing the energy barriers of 12.8 and 13.0 K, respectively. To further improve their energy barriers, one strategy is to introduce multidentate ligands and 4d-block metallo-cyanate with stronger magnetic anisotropy.

## References:

- [1] Sessoli R, Tsai H L, Schake A R, et al. *J. Am. Chem. Soc.*, **1993**,**115**:1804-1816
- [2] Sessoli R, Gatteschi D, Caneschi A, et al. *Nature*, **1993**,**365**: 141-143
- [3] Wernsdorfer W, Aliaga-Alcalde N, Hendrickson D N, et al. *Nature*, **2002**,**416**:406-409
- [4] Corrales S A, Cain J M, Uhlig K A, et al. *Inorg. Chem.*, **2016**, **55**:1367-1369
- [5] Leuenberger M N, Loss D. *Nature*, **2001**,**410**:789-793
- [6] Liu R N, Li L C, Wang X L, et al. *Chem. Commun.*, **2010**,**46**: 2566-2568
- [7] Milios C J, Inglis R, Vinslava A, et al. *J. Am. Chem. Soc.*, **2007**,**129**:12505-12511
- [8] Bogani L, Wernsdorfer W. *Nat. Mater.*, **2008**,**7**:179-186
- [9] Mannini M, Pineider F, Saintavitt P, et al. *Nat. Mater.*, **2009**, **8**:194-197
- [10] Qian K, Huang X C, Zhou C, et al. *J. Am. Chem. Soc.*, **2013**, **135**:13302-13305
- [11] Pedersen K S, Bendix J, Clérac R. *Chem. Commun.*, **2014**, **50**:4396-4415
- [12] Li D F, Parkin S, Wang G, et al. *J. Am. Chem. Soc.*, **2006**, **128**:4214-4215
- [13] Wang C F, Zuo J L, Bartlett B M, et al. *J. Am. Chem. Soc.*, **2006**,**128**:7162-7163
- [14] Li D F, Clérac R, Parkin S, et al. *Inorg. Chem.*, **2006**, **45**: 5251-5253
- [15] Li D F, Parkin S, Clérac R, et al. *Inorg. Chem.*, **2006**, **45**: 7569-7571
- [16] Zhang Y Z, Mallik U P, Rath N, et al. *Chem. Commun.*, **2010**,**46**:4953-4955
- [17] Wang S, Ding X H, Zuo J L, et al. *Coord. Chem. Rev.*, **2011**, **255**:1713-1732
- [18] Zhang Y Z, Mallik U P, Clérac R, et al. *Chem. Commun.*, **2011**,**47**:7194-7196
- [19] Beltran L M C, Long J R. *Acc. Chem. Res.*, **2005**,**38**:325-334
- [20] Li D F, Parkin S, Wang G B, et al. *Inorg. Chem.*, **2005**,**44**: 4903-4905
- [21] Aguilà D, Prado Y, Koumoussi E S, et al. *Chem. Soc. Rev.*, **2016**,**45**:203-224
- [22] Li D F, Parkin S, Wang G B, et al. *Inorg. Chem.*, **2006**,**45**: 1951-1959
- [23] Gatteschi D, Sessoli R. *Angew. Chem. Int. Ed.*, **2003**,**42**:268-297
- [24] Ruamps R, Maurice R, Batchelor L, et al. *J. Am. Chem. Soc.*, **2013**,**135**:3017-3026
- [25] Zhuang P F, Zhang Y J, Zheng H, et al. *Dalton. Trans.*, **2015**, **44**:3393-3398
- [26] Rebilly J, Mallah T. *Single-Molecule Magnets and Related Phenomena*. Winpenney R. Ed., Berlin, Heidelberg: Springer, **2006**:103-131
- [27] Lescouëzec R, Vaissermann J, Lloret F, et al. *Inorg. Chem.*, **2002**,**41**:5943-5945
- [28] Zhuang P F, Luo L, Liu T, et al. *Inorg. Chem. Commun.*, **2014**,**48**:8-11
- [29] SMART, SAINT and XPREP, Area Detector and Integration and Reduction Software, Bruker Analytical Instruments Inc., Madison, WI, **1995**.
- [30] Sheldrick G M. *SHELXS-97, Program for X-ray Crystal Structure Solution and Refinement*, University of Göttingen, Germany, **1997**.
- [31] Dolomanov O, Bourhis L, Howard J, et al. *J. Appl. Crystallogr.*, **2009**,**42**:339-341
- [32] Wu D Y, Zhang Y J, Huang W, et al. *Dalton. Trans.*, **2010**, **39**:5500-5503
- [33] Pardo E, Verdaguer M, Herson P, et al. *Inorg. Chem.*, **2011**, **50**:6250-6262
- [34] Zhang Y Z, Mallik U P, Clérac R, et al. *Polyhedron*, **2013**,**52**: 115-121
- [35] Jiao C Q, Jiang W J, Wen W, et al. *Inorg. Chem. Commun.*, **2016**,**74**:12-15
- [36] Hu J X, Zhang Y J, Xu Y, et al. *Inorg. Chem. Commun.*, **2014**,**47**:155-158
- [37] Liu W, Wang C F, Li Y Z, et al. *Inorg. Chem.*, **2006**, **45**: 10058-10065
- [38] Li D F, Clérac R, Wang G B, et al. *Eur. J. Inorg. Chem.*, **2007**:1341-1346
- [39] Wang C F, Liu W, Song Y, et al. *Eur. J. Inorg. Chem.*, **2008**: 717-727
- [40] Liu X R, Jiao C Q, Meng Y S, et al. *Z. Anorg. Allg. Chem.*, **2019**,**645**:428-432
- [41] Jiao Y S, Jiao C Q, Meng Y S, et al. *Inorg. Chem. Commun.*, **2018**,**93**:87-91